JOURNAL OF GEOPHYSICAL RESEARCH, VOL. ???, XXXX, DOI:10.1029/,

The upper ocean circulation and water masses in the western PIRATA sites from 1999 to 2005

D. F. Urbano,[1] P. Nobre,[1]

D. F. URBANO, Divisão de Modelagem e Desenvolvimento, Centro de Previsão de Tempo e Estudos Climáticos, Instituto Nacional de Pesquisas Espaciais (CPTEC/INPE), Rodovia Presidente Dutra KM40, Cachoeira Paulista, SP, 12630-000, Brazil. (dfurbano@cptec.inpe.br)

[1]Instituto Nacional de Pesquisas Espaciais
(INPE), Cachoeira Paulista, São Paulo,
Brazil.

Abstract.

Simultaneous direct velocity measurements (shipboard ADCP) and hydrographic data ($CTDO_2$) are used to investigate the upper ocean circulation and water masses distribution in the western tropical Atlantic. Seven vertical sections along 38°W from the South American coast to 15°N were taken from 1999 to 2005 as part of the Pilot Research Moored Array in the Tropical Atlantic (PIRATA) program. An Equatorial Undercurrent (EUC) multicore structure is described, suggesting a complex feeding process at this longitude. Two main EUC cores lie above and below the 20°C surface, respectively. Strong observational evidence of thermocline ventilation is found in both EUC and North Equatorial Undercurrent (NEUC) regions. Salinity-oxygen analysis suggests that subtropical high salinity water from the North Atlantic is carried by one of the EUC cores. The North Equatorial Countercurrent (NECC) was measured from 3°N to 14°N. The second branch of the NECC (nNECC) lies between 8°N and 14°N, and carries both North and South Atlantic waters. The nNECC was recently measured in the eastern tropical Atlantic but was never directly measured in the western part of the basin. In most of the PIRATA cruises analyzed, the two NECC cores are 3° to 4° apart from each other. During July 2003, the two cores were found to be connected with no westward flow between them. Astonishingly, the July 2004 cruise captured the exact moment in which the nNECC detaches from the sNECC to migrate northward. No NECC reversal was detected during any of the winter and spring cruises, supporting previous numerical model

research showing that this current never reverses direction, presenting only an intensification and change in direction of the Ekman flow due to the ITCZ displacement.

1. Introduction

The tropical Atlantic Ocean has been intensely investigated since the 1960's when the ETAMBOT I and II observational programs were carried out [*Austin*, 1963; *Cochrane*, 1963; *Metacalf and Staculp*, 1967; *Luedemann*, 1967; *Metacalf*, 1968]. During the 1970's and 1980's, the Global Atmospheric Research Program (GARP) - Atlantic Tropical Experiment (GATE), *François Océan Climat Atlantique Equatorial* (FOCAL), and the Seasonal Response of the Equatorial Atlantic Experiment (SEQUAL) were the main observational programs. A collection of 24 articles in Geophysical Research Letters, volume 11, number 8, August 1984 concentrates the first year of results from the FOCAL/SEQUAL two-year joint program. Reprints from the Journal of Geophysical Research, volumes 91 and 92 collect more observational and modeling articles from these programs. During the 1990's, the western tropical Atlantic was the research target due to the inter-hemispheric mass and heat budget. The Western Tropical Atlantic Experiment (WESTRAX) [*Brown et al.*, 1992] provided one of the first acoustic profiler velocity measurements in the region through the Pegasus system. The World Ocean Circulation Experiment (WOCE) supplies a large number of large-scale observational data all around the world. However, there is still a need for high-resolution observational data that covers the whole tropical basin and that continually collects information throughout the year for a long time period (decades). The lack of oceanic and atmospheric data in the tropics limits our ability to make progress on important climate issues. Therefore, the Pilot Research Moored Array in the Tropical Atlantic (PIRATA) [*Servain et al.*, 1998] attempts to address this lack of data. The PIRATA Autonomous Temperature Line Acquisition System (ATLAS) moor-

50 ings are transmitting meteorological and oceanic measurements via satellite in real time
51 since 1998, similar to the Pacific TAO program.

52 In the past, much of the knowledge on ocean circulation was obtained from maps of
53 geostrophic velocity computed indirectly from temperature, salinity, and pressure: the
54 Dynamic Method. However, there are well known technical limitations, mainly in the
55 equatorial and boundary regions. The numerical modeling, still indirect but much more
56 powerful, provides relatively good multidimensional velocity maps. However, nowadays
57 neither analytical nor numerical methods are able to supply velocity with the desired level
58 of details. Therefore, direct ocean velocity measurements, which nowadays use acoustic
59 systems, are essential for understanding ocean dynamics.

60 Besides the high-resolution time series from the ATLAS buoys, high-resolution vertical
61 profiles of ocean velocity, temperature, and salinity (and dissolved oxygen after 2003) have
62 been measured along 38°W during PIRATA oceanographic cruises once a year. The ship
63 data complete the buoys information since they are important when drawing a picture
64 of the upper circulation at a given location and time. Near 38°W, where the western
65 PIRATA buoys are strategically deployed, only a few direct velocity measurements had
66 been done up to 8°N and none northward this latitude. Thus, the PIRATA direct velocity
67 observations (and CTD) are novel observations that supply a fresh view of the 38°W
68 meridian from the South American coast to 15°N (Figure 1). The main goal of this
69 work is to present additional descriptions of the upper layer currents and water mass
70 distribution at the western PIRATA sites.

71 This text is organized as follows. The next Section describes the data sets. Section 3.1
72 presents the water masses distribution while Section 3.2 discuss the upper ocean circu-

lation, describing the main currents. Section 3.3 presents additional analysis using the combined velocity, salinity and dissolved oxygen vertical maps. Section 4 summarizes the main ideas.

2. Data

The data set used in this study is part of the Pilot Research Moored Array in the Tropical Atlantic (PIRATA), a multi-national cooperation Program [*Servain et al.*, 1998]. Since 1998 oceanographic surveys have been conducted by the Brazilian effort once a year for maintenance of the Autonomous Temperature Line Acquisition System (ATLAS) moorings, shown in Figure 1. Underway shipboard Acoustic Doppler Current Profiler (ADCP) data were collected, Conductivity-Temperature-Depth (CTD) sensors were cast, and Expendable Bathythermograph (XBT) probes were released. The track lines and CTD locations for the seven cruises considered herein are shown in Figure 1. The tracks, dates, and data types for each cruise are summarized on Table 1. The timing of the cruises was dictated primarily by the mooring battery time-life and by vessel availability rather than by scientific considerations. However, effort was expended to match the cruise dates with the southernmost Inter-tropical Convergence Zone (ITCZ) position due to its relevance to the South American rainfall.

2.1. Shipboard ADCP

Velocity was measured by a 75-kHz vessel-mounted ADCP from RD Instruments on board the Brazilian Navy R/V Antares. The data were collected continuously along the cruise tracks along 38°W (Figure 1), from 1999 to 2005 (Table 1). These ADCP data are novel observations in the western tropical Atlantic since the track-lines reach 15°N at this

longitude. There is only a limited set of observations beyond 5°N around this longitude [*Arhan et al.*, 1998; *Bourlès et al.*, 1999a, b, 2002].

The seven PIRATA ADCP data sets were named Transect or VM-DAS according to the employed data acquisition software (Table 1). The processing and calibration of the obsolete Transect data are difficult and this raw data type is no longer recommended nor supported. The raw data were collected using a vertical bin length of 8 m with the first reliable bin representing a velocity mean from 16 to 24 m in depth. The depth range was about 400 m but it is dependent on sea state; the range was less than 250 m when the ship headed into heavier weather.

The data were processed and calibrated using the Common Ocean Data Access System (CODAS) developed and maintained by a group of the University of Hawaii [*Firing et al.*, 1995]. The original 5-min mean values have been processed and further averaged into 1/4° horizontally. ADCP absolute current was determined by using standard shipboard gyroscopic compass heading and navigation from the Global Positioning System (GPS). The accuracy of the mean velocity profiles was estimated to be better than 5 cm s^{-1}.

2.2. $CTDO_2$

Hydrographic data were collected with a SeaBird SBE 9Plus CTD instrument at each degree of latitude along 38°W (Figure 1). The CTD profiles along the cruise track were 500-m in depth but restricted to 300 m and to the north of 4°N for the first cruise (JAN1998), and restricted to the ATLAS sites for the last two cruises (JUL2004 and JUL2005). Instead of 11.5°N, the ATLAS system was deployed at 12°N on FEB1999. Due to the restrictions in January 1998, this cruise was not used here.

During APR2002 and JUL2003, the CTD casts were simultaneous to the ADCP profiles while during the other cruises there is a time lag of a few days, preserving however, the synopticity. For this study, ATLAS and XBT data were used to fill out the CTD salinity and temperature gaps, when available. At the ATLAS sites the CTD profiles were deeper, reaching levels between 1000-m depth and the local bottom.

The conductivity, pressure, and temperature sensors were calibrated before each cruise. Additional calibration was provided by in situ water samples (Nansen bottles) at standard depths and by thermosalinograph data. Duplicity of sensors was used when available as a means of quality control. Dissolved oxygen sensors were installed on the CTD system after 2003 and water samples were used for calibration.

3. Water Masses and Upper Circulation

A 7-year series of vertical sections of ADCP and CTD data, as summarized on Table 1, is presented (Figures 3 to 5). Figure 2 displays the water masses configuration along 38°W during July 2003. Superimposed are the 20°C and 27°C isotherms, commonly used to represent the thermocline position and the mixed layer lower boundary, respectively (thick gray lines). The 24.5 Kg m^{-3} and 26.75 Kg m^{-3} density surfaces determine the top and bottom of the pycnocline (thick black lines).

Figures 3 to 5 display velocity sections of the upper zonal current system at 38°W and, on the right of each map, the correspondent Theta-S diagram. On top of the velocity maps, circles mark the CTD stations and triangles point to the ATLAS sites (See Figure 1 for horizontal distribution). Besides temperature and density, the salinity was overlaid (thin black lines). The Theta-S diagrams were computed from the CTD casts at the ATLAS sites along 38°W and on the equator when available (see section 2.2 for details). The two

upper density surfaces plus the 27.1 Kg m^{-3}, as the Intermediary Layer lower limit, were included.

Analyzing velocity, salinity and temperature together is essential in order to understand water mass origin and current pathways.

3.1. Water Masses

The water mass distribution in the tropical Atlantic has been recently investigated [*Wilson et al.*, 1994; *Stramma et al.*, 2005a, b] and a good review is found in *Stramma and Schott* [1999]. Therefore, a brief description is presented here.

Different water masses are well identified along 38°W up to 15°N (Figure 2 and Figures 3 to 5). The Tropical Surface Water (TSW) with temperatures of about 27°C forms the mixed layer, therefore lying above the 24.5 density layer (Figure 2). Underneath, the Atlantic Central Water is characterized by a linear Theta-S relationship, and is located between the 27.1 density layer and the thermocline (20°C) (Figures 3 to 5). The South Atlantic Central Water (SACW) is fresher and warmer (and contains less dissolved oxygen) than the North Atlantic Central Water (NACW), therefore a separation between the two can be seen clearly by the salinity front north of 10°N (Figure 2) and in the Theta-S diagrams (Figures 3 to 5). Low salinity (36 to 36.25) and high temperature (20° to 25°C) characterize the eastern TSW, which lies above the SACW and re-circulates in the tropical Atlantic into the zonal current system. The atmospheric convective process, i.e. rainfall, associated with the Atlantic ITCZ affects the TSW characteristics due to the large input of fresh water. The Salinity Maximum Water (SMW), also called Subtropical Underwater, is characterized by salinity maximum at densities around 24.5 and 25 Kg m^{-3}. The

SMW is formed in the tropics-subtropics transition region by subduction and progresses equatorward as a subsurface salinity maximum, ventilating the tropical thermocline.

The salinity front between the SACW and the NACW extends zonally across the entire North Atlantic Ocean from the Caribbean Sea to the African coast [*Onken and Klein*, 1991]. Its eastern part, The Cape Verde Frontal Zone (CVFZ), has been intensively investigated [*Onken and Klein*, 1991; *Spall*, 1992; *Klein and Siedler*, 1995; *Lozier et al.*, 1995; *Vangriesheim et al.*, 2003]. This frontal system is an effective barrier between different water masses rather than a blender; water exchange most likely takes place as the result of large-scale horizontal instabilities which are responsible for the high temporal variability in the frontal position [*Perez-Rodriguez et al.*, 2001].

3.2. Velocity Field

An overview of the mean flow field and its fluctuations was given by *Stramma and Schott* [1999], which includes the direct velocity descriptions of *Schott et al.* [1995] and *Schott et al.* [1998]. Focused on the warm water formation and escape process, *Lee and Csanady* [1999] review current understanding in the tropical Atlantic. An extensive analysis of the currents in the equatorial west Atlantic was presented by *Bourlès et al.* [1999a]. The mean pathways and volume transports in the pycnocline and surface layer for water flowing between the subtropical and tropical Atlantic Ocean (Subtropical-Tropical Cells; STC) was recently determined through climatological observations by *Zang et al.* [2003]. Therefore, there is a relatively detailed description of the western tropical Atlantic circulation. However, *Zang et al.* [2003] emphasizes the lack of measurements in the North Atlantic STC region; an important key process for climate understanding. At 38°W, only a few direct velocity measurements were collected up to 8°N. The PIRATA program provides novel

direct velocity measurements north of 8°N and up to 15°N which will be described here. Transports of the main upper currents were computed and are presented on Table 2.

3.2.1. The EUC

Between 2°S and 3°N, the Equatorial Undercurrent (EUC) depicts an eastward multiple core structure above the 26.75 density layer, with two well defined cores within the pycnocline (Figures 3, 4, and 5). A close up on the EUC region is shown on Figure 6. *Schott et al.* [1995] describes two eastward cores in the EUC at 40°W during March 1994. No dynamical explanation was given regarding the double core existence. They also mention that no North Atlantic water was carried by the cores at that time. *Goes et al.* [2005] examined velocity sections at 44°W, 41°W, and 35°W from a cruise conducted in February 2002. The authors demonstrate that the single EUC core at 44°W and 41°W separates into the NEUC and EUC by 35°W, with the former composed of northern hemisphere waters and the latter southern hemisphere waters. These results indeed point to a very complex EUC behavior at 38°W.

The southernmost and deeper EUC core is located mainly between 1°S and the equator, and always below the 20°C. Figure 6 shows that the 20°C is always between the two main EUC cores. They must therefore have distinct water mass origins and dynamics. This southern EUC core carries water with salinity fresher than 36, typically eastern Atlantic waters. This low-salinity water originates from the eSEC bifurcation in the western Atlantic [*Bourlès et al.*, 1999b]. The second EUC core is on top of the thermocline, shifted slightly northward, and is always above the 20°C layer (Figures 3 to 6). During MAR2000, APR2001, and APR2002, there is an inflection on the 24.5 line around 1.5°N associated with this northern core intensification (Figures 3 and 4). This core coincides in position

with high salinity patches of values greater than 36.25. This is a strong observational evidence for the thermocline ventilation process where subducted high salinity subtropical waters flow equatorward to feed the zonal current system [*Lazar et al.*, 2002; *Zang et al.*, 2003].

An extra subsurface core between the surface and the 27°C layer was measured during the winter. During FEB1999, despite the lack of profiles, a subsurface core about 45 cm s^{-1} was measured near 2°N. During MAR2000, this feature was found at 4°N and has about 10 to 20 cm s^{-1}, being almost detached from the EUC but connected to the NEUC (Figure 3). An eastward near-surface flow with velocities of up to 40 cm s^{-1} above the EUC have already been observed, as discussed by *Bourlès et al.* [1999b]. The authors mention that a possible explanation for this flow is the near-equatorial location of the ITCZ that leads to a relaxation of the wind forcing and an eastward pressure gradient. However, an eastward flow above the EUC was observed around 2°S in September 1995 and during two October cruises described by *Schott et al.* [1998], time in which the ITCZ has its northernmost position. Another possible explanation for this feature was the influence of the vertical advection of eastward momentum in the presence of large mean shear on the east component fluctuations. *Bourlès et al.* [1999b] also mention that works using numerical experiments explain the presence of this flow in the numerical results due to the weakness of the vertical viscosity coefficient used in the model.

During MAR2000, APR2001, and APR2002, the EUC is shallower and more intense (Figures 6b, 6c, and 6d). The core velocity is over 100 cm s^{-1} and the transport during APR2001 is 31.8 Sv (1Sv=1×10^6 Kg m^{-3}; Table 2). No velocity was measured above 24 m depth, but the data suggest that the EUC reaches the surface during these cruises. During

July cruises (Figures 6e, 6f, and 6g), the EUC is deeper (around 150 m depth). During JUL2003 and JUL2004, this current is relatively weaker (75 cm s^{-1}) with no connection with the surface during JUL2004. Otherwise, during JUL2005, this current is strong (95 cm s^{-1}). JUL2005 seems to be an anomalous event, suggesting therefore a strong inter-annual variability. It is important to remember here that the JUL2004 section was taken diagonally from 38°W,15°N to 35°W,3°S. During this cruise the EUC is mostly at and southward of 35°W.

The data set described here has no measurements during the fall season and, therefore, does not allow for an appropriated seasonal cycle investigation. *Arhan et al.* [2006] analyze the annual cycle of the EUC using a realistic ocean general circulation model and compare the results with observations. The authors describe two well defined transport maxima along the year: one during summer and fall and a second, most pronounced near the western boundary, during April-May. The intensified March and April EUC described here agrees well with the model results.

3.2.2. The nSEC and NECC

North of 2°N and above the thermocline, there are the two opposite currents directly driven by the wind: The northern branch of the South Equatorial Current (nSEC) and the North Equatorial Countercurrent (NECC). Both currents exhibit a strong seasonal cycle associated with the ITCZ meridional displacement [*Katz and Garzoli*, 1984; *Katz*, 1987; *Garzoli*, 1992].

The nSEC carries surface fresh and hot water from the eastern tropical Atlantic, with salinity fresher than 36 and temperatures warmer than 27°C. Its westward flux is weak during the winter cruises, with a maximum westward velocity of -25 cm s^{-1} at 3°N during

FEB1999. This current is limited to regions above 70 m depth and between 2°N and 5°N during this cruise. During MAR2000 its core is at 5°N but there is also a westward flow at 3°N and 120 m depth. The transports are -1.1 Sv for FEB1999 and -2.5 Sv for MAR2000 (Table 2). During the spring cruises, the nSEC is a broad current between 2°N and 8°N with a surface core of -45 cm s^{-1} and transports about -7.5 Sv for APR2001 and -14.3 Sv for APR2002. During summer cruises, the nSEC lies southward and centered at 2°N, with the core velocity higher than -80 cm s^{-1}. A stronger westward transport of -17.3 Sv is observed during JUL2003. During JUL2005, the nSEC zonal component is weaker compared with the other July cruises, and its transport is only -4.8 Sv. At the same time, the EUC is intensified, probably related to an abnormal relaxation on the trade winds this year.

The NECC, for a long time and due to the lack of direct velocity measurements, was improperly defined as the eastward surface flow (1) lying between 3°N and 8°N, (2) that is fed by South Atlantic waters only, and (3) that reverses direction during spring seasons. In a recent work, *Urbano et al.* [2006] show that the NECC lies between 3°N and 13°N, and that new observational programs should extend the measurements north of 8°N which might then be used in new NECC heat, mass, and vorticity budget analysis. The authors also show that the NECC has a second northward core between 8°N and 13°N through the year; we will return to this important subject later on in this text. The velocity sections presented here, Figures 3 to 5 and Figure 7 clearly show the NECC extending north of 8°N. During APR2002 (spring), the NECC is completely north of 8°N while the nSEC is located between 2°N and 8°N. Regarding (2), previous work [*Mayer and Weisberg*, 1993; *Bourlès et al.*, 1999a, b] had already showed that the NECC is fed by both the NBC retroflection

and by the North Equatorial Current (NEC), the southern limb of the subtropical North Atlantic gyre. The simultaneous ADCP, salinity and dissolved oxygen data disposed in vertical maps (Figure 8) show that the NECC is fed by both Northern and Southern Hemispheric waters (See Section 3.3 for oxygen analysis). Regarding (3), *Bourlès et al.* [1999a] show trough ADCP and $CTDO_2$ data that the NECC was present in boreal spring (April-May 1996) west of 40°W, fed with water of Northern Hemisphere origin only. The ADCP sections presented here (Figure 3) show that the NECC was also present in both boreal spring of 2001 and 2002, north of 7.5°N. *Jochum and Malanotte-Rizzoli* [2003] showed through model results that the NECC never reverses direction and that only the Ekman layer becomes stronger and changes direction. Therefore, the novel direct velocity PIRATA measurements together with previous results provide strong evidence to settle this old NECC definition.

Urbano et al. [2006] rediscovered the nNECC at 35°W but the second core has never been observed directly. Recent direct velocity data in the eastern Atlantic [*Stramma et al.*, 2005a] displays the NECC double core structure. However, the PIRATA ADCP data are the first direct velocity observation in the western Atlantic that measured the second core of the NECC. *Urbano et al.* [2006] described that these features are in Sverdrup balance; they must therefore be generated by the particular structure of the wind field. Consequently, the two cores of the NECC are the direct result of the finite width of the ITCZ, which has two curvature maxima of the zonal wind stress. The distance between the cores is directly proportional to the width of the ITCZ. A good picture that describes the nNECC seasonal behavior was presented by *Urbano et al.* [2006], their Figure 6.

Figure 7 presents the positive velocities only in the NECC region and for all PIRATA cruises. During the winter (i.e. FEB1999 and MAR2000; Figures 7a and 7b), the NECC displays the two-core structure 3° to 4° apart from each other. During FEB1999, the sNECC reaches 40 cm s^{-1} at 7°N and 80 m depth, while the nNECC has 20 cm s^{-1} from 24 to 70 m depth. Both cores together account for 10.5 Sv (see Table 2). During MAR2000, the sNECC has 30 cm s^{-1} at 7°N extending from 24 to 110 m depth, while the nNECC has a subsurface core of 10 cm s^{-1} at 12°N. The total transport is 7.4 Sv.

During spring (i.e. APR2001 and APR2002; Figures 7c and 7d), the ITCZ reaches its climatologically southernmost position and the NECC has the lowest transport value of the seasonal cycle. It is not clear, from the observational evidence analyzed so far, whether the nNECC remains at that time. However, based on the temperature and salinity information shown in Figure 7, it is possible to infer that the NECC depicts a weak main core at 7°N and up to 40 m depth. The 27°C and 36 psu lines outcrop the surface contouring the southern core. Near 8°N, a subsurface core of 10 cm s^{-1} can be associated with the nNECC. During APR2002, a nNECC of 10 cm s^{-1} is identified around 11°N and at 50 m depth, extending below 120 m. The sNECC shows a 40 cm s^{-1} core at 9°N, but it is restricted between 8°N and 10°N (Figure 7d), with an eastward transport of 4 Sv.

During summer (i.e. July cruises; Figures 7e, 7f, and 7g), the NECC presents different features. When the sNECC and nNECC are close, it is difficult to identify the nNECC. However, the deep structure often associated with the northern core reveals its presence (see Figure 5 for deep structure). During JUL2003 (Figure 7e), the sNECC is stronger, with a subsurface core of 100 cm s^{-1} at 6.5°N and 60 m depth. The nNECC is also stronger,

with 30 cm s^{-1} between 40 and 80 m depth. At this time, the NECC has its strongest transport (17.9 Sv) of all cruises presented here. The JUL2004 map (Figure 7f) shows a very important phase of the nNECC; this transect depicts the moment in which the nNECC apparently starts to detach from the sNECC to go back to its original position at 11-12°N. The sequence of events shown by Figure 7 agrees well with the nNECC position in the climatological seasonal cycle of transport presented by *Urbano et al.* [2006], their Figure 6. The sNECC has 60 cm s^{-1} at 5°N and 70 m depth, and the total NECC transport was 9.8 Sv. During JUL2005, the sNECC core is 70 cm s^{-1} at 6.5°N and around 60 m depth. Alone, the sNECC transport is 11.4 Sv. During JUL2005 the nNECC (Figure 7g) is evident but its full development is expected to happen in September-October, as presented by *Urbano et al.* [2006]. Unfortunately, there are no measurements during these months. The nNECC reached 20 cm s^{-1} at 110 m but was not stronger than 10 cm s^{-1} at 70 m and at 30 m depth (Figure 7g). Alone, the nNECC transport is 2.8 Sv (Table 2).

3.2.3. The NEUC

In pycnocline levels and between 3°N and 7°N, the eastward North Equatorial Undercurrent (NEUC) [*Molinari et al.*, 1981] is associated with an evident slope on the 26.75 density layer north of 4°N in all cruises but FEB1999 (Figures 3 to 5). However, this density surface cannot determine the NEUC lower limit since there is an eastward flow below this surface. During the winter (Figure 3), the NEUC was connected with both EUC and NECC; it was isolated during spring (Figure 4), and connected only with the NECC during the summer cruises (Figure 5). On top of the NEUC, similarly to the EUC, another patch of high salinity is found. It suggests that the NEUC is also fed by subtropical water through thermocline ventilation.

In FEB1999 (Figure 3), the maximum velocity is 50 cm s^{-1} centered at 5°N and 150 m depth. Its transport is 8.9 Sv (Table 2). During MAR2000, the NEUC reaches 35 cm s^{-1} at 4°N, and its transport is 5.6 Sv. The shallower ADCP sampling during APR2001 (Figure 4) renders inconclusive the determination whether the NEUC core is as weak as 10 cm s^{-1}, or wether it is deeper than the 130 m depth sampled. However, during APR2002, the NEUC also has a weak core of 10 cm s^{-1} centered at 5°N. The transport during this two spring cruises are only 0.7 and 1.0 Sv, respectively (Table 2).

During the summer, the NECC is displaced southward and aligned with the NEUC (Figure 5). The NEUC core is added to the NECC eastward flow. During JUL2003 and JUL2005, the NEUC is centered at 5°N, above the 24.5 density layer, and south of the NECC. During both cruises the core velocity is 30 cm s^{-1}, and the transports are 3.4 and 5.4 Sv, respectively. In JUL2004, the NEUC is northward of the NECC, centered at 6°N, and is part of the eastward flow usually associated with the nNECC deep structure. Its transport is 3.6 Sv.

Even though connected with the NECC and EUC, the NEUC core is below the thermocline, and therefore it is commonly assumed that this current cannot be directly wind-driven. However, the dynamics regarding both north and south Equatorial undercurrents, in the Atlantic and Pacific oceans, is still not completely understood. There are two hypothesis: *McCreary et al.* [2002] suggest that the undercurrents are driven by off-equatorial upwelling and that they are an essential branch of the thermo-haline circulation. *Jochum and Malanotte-Rizzoli* [2004] suggest that in addition to the *McCreary et al.* [2002] mechanism, there is the Eliassen-Palm flux of the Tropical Instability Waves (TIWs). It is the particular structure of the TIWs that leads to maxima in the convergence of the

Eliassen-Palm flux at approximately 4°N (5°S), thereby determining the position of the undercurrent.

It is important to mention that the NEUC transport computation is difficult due to its proximity to both the EUC and the NECC. Besides, the lower integration limit used here for the NEUC transport computation was only 250 m and the acoustic profiles did not reach this depth in all cruises.

3.3. Dissolved Oxygen Analysis

The upper water column in the western tropical Atlantic has not only distinctive temperature-salinity correlation but also temperature-oxygen and salinity-oxygen correlation, which can be used to infer more details about the origins of regional water masses [*Wilson et al.*, 1994]. However, extra care must be taken since dissolved oxygen is a non-conservative property. PIRATA $CTDO_2$ stations at each degree of latitude from the PBR06 cruise (JUL2003) allow us to combine the oxygen concentration with salinity and velocity (Figure 8) to better understand the upper circulation along 38°W.

Figure 8a displays the vertical section of dissolved oxygen with concentrations higher than 3.5 ml l^{-1} shaded. For this cruise, the concentration range is narrow, being between 3 and 4 ml l^{-1}. Usually subtropical waters have oxygen concentration of 4 to 5 ml l^{-1}, while typical deep and poor oxygen waters have less than 2 ml l^{-1}.

Subtropical North Atlantic water is found north of 11°N, on pycnocline levels and associated with the SMW which sinks northward of 15°N. This water is associated with the NEC (see Figures 8b and 8c for velocity and Figure8c for salinity). For JUL2003, as for FEB1999, the maximum salinity value associated with the SMW is 36.75 while for all the other cruises the salinity maximum is over 37 psu (Figures 3 to 5). The

high variability and intense eddy activity there probably mixed the waters leading to lower salinity values. Also, Figures 8b and 8c, the zonal and meridional velocity fields respectively, display several changes in flow direction at this depth. Another reason for the lack of higher salinity at 15°N at those cruises is the NECC northward displacement, which restrains the penetration of SMW equatorward.

Between 2°N and 11°N, and above 100 m, there are three regions of low oxygen concentration (Figure 8a). South of 1°N, both the eSEC and the upper EUC carry high salinity (36 to 36.5 psu) and relatively low oxygen water (3.4 to 3.5 ml l^{-1}). From the meridional velocity field (Figure 8c) both the eSEC and the upper EUC show a southward component. The eSEC water is flowing southwestward before joining the northwestward NBC/NBUC system and turning anti-cyclonicaly to feed the EUC west of 38°W. [*Zang et al.*, 2003] show through climatological data that the EUC is ventilated by South Atlantic subtropical water both through a western boundary route (NBC/NBUC) and an interior route across 6°S, between the western boundary and 10°W. The high salinity water found here within the eSEC is probably from the interior route.

The northwestward nSEC (1°N to 5°N) carries relative high oxygen waters (over 3.5 ml l^{-1}). Salinity higher than 36 is found in subsurface levels, while low salinity is found above 75 m, probably due to heavy equatorial rainfall activity. [*Zang et al.*, 2003] suggest that the high-salinity water of North Atlantic origin flows westward in the NEC, skirting the region of high potential vorticity under the ITCZ, then flows southward and southeastward into the NECC (see Figure 8). Part of these waters, along with South Atlantic waters retroflected from the NBC, may upwell along the path of the NECC in the upwelling regions under the ITCZ and near the African coast. Some of these waters may also become

entrained into the westward nSEC and then be drawn into the EUC. These serpentine pathways are consistent with the numerical modeling results of *Malanotte-Rizzoli et al.* [2000] and *Inui et al.* [2002], and with the features presented in Figure 8.

At 6°N and 9°N, the sNECC and nNECC, similarly to the upper EUC, are fed by low oxygen, but very fresh (35.25 to 36), water. In most likelihood, strong rainfall activity associated with the ITCZ and the Amazon River runoff contribute to the surface low salinity in this region.

Two cores of low oxygen are found north of 8°N and below 100 m depth. These two low oxygen regions are associated with two well-defined northwestward flows at 10°N and 14°N (Figures 8b and 8c). The southern core is fresher and has less dissolved oxygen (35 psu and 3 ml l^{-1}) than the core north of the front (35.75 psu and 3.2 ml l^{-1}). Waters from the Guinea Dome upwelling (10°N, 23°W), which have low oxygen, join the NEC north and south of the Cape Verde Island to form the CVFZ and flow westward [See *Stramma and Schott* [1999], their Figure 4].

4. Summary

Additional information about the upper ocean circulation is provided using direct velocity measurements and hydrographic observations from annual PIRATA cruises along 38°W and from 1999 to 2005. The velocity data described here are novel observations since the meridional sections extended up to 15°N while the previous few direct velocity data northernmost latitudes reached up to 7.5°N.

The EUC multiple core structure is described. Strong observational evidence of thermocline ventilation is given by high salinity, apparently from the North Hemisphere, associated with the northernmost EUC core. This core is frequently found on the top of

the thermocline while the southern core is below 20°C. Whether the high salinity water is from the South or North Hemisphere can only be defined through lagrangian analysis and high-resolution model experiments. Observational evidence of thermocline ventilation in the NEUC region is also provided by the PIRATA data. An important contribution of the seven PIRATA velocity sections is that the EUC multiple core structure at 38°W shows itself to be much more complex then thought and that 38°W is a key region for the understanding of thermocline ventilation and therefore climate.

One of the most important results of this work is the direct measurement of the NECC northern branch (nNECC). In a recent paper, *Urbano et al.* [2006] rediscovered the NECC second core but the strongest observational evidence of this feature was only found, at that time, in ship-drift and surface drifter data. Until the PIRATA ADCP data, the NECC second core had never been observed directly in the western tropical Atlantic. *Urbano et al.* [2006] suggested a dynamical mechanism driving the NECC cores and presented a climatological picture of the seasonal cycle of transports computed from the QuikSCAT data. In that picture, the NECC cores are 4° apart from each other from January to May. In June-July-August, the cores are connected due to the northernmost ITCZ position. In September, the second core has its strongest transport and the cores are again 4° apart. In November-December the seasonal cycle starts again. The seven PIRATA velocity maps did not completely fill the seasonal cycle, but were able to register the different phases of the nNECC, supporting the climatological description.

For a long time, the NECC was thought to be the eastward flow between 3°N and 8°N, only fed by South Atlantic waters through NBC retroflection. As no retroflection can occur during spring, it was also thought that the NECC reverses direction during

that time, mainly during April. The PIRATA observations, together with previous recent results, present strong observational evidence that the NECC does not actually reverse direction. During the two spring cruises presented here (APR2001 and APR2002), the NECC is weak and caries both North and South Atlantic waters. Therefore, the PIRATA observations supply strong evidence to settle the old NECC definition.

The water mass distribution along 38°W had been extensively described and reviewed by previous works. Therefore, few new information was added and most of the features described here are in agreement with previous findings. Otherwise, the simultaneous $CTDO_2$ and ADCP maps shed light on the currents feeding processes, mainly about the NECC. The dissolved oxygen observations described here, even though limited to one cruise (JUL2003), were essential in order to support the idea that the NECC is indeed fed by both South and North Atlantic waters, and that there is strong variability on this feeding process, with strong eddy activity between the NECC and NEC superimposed on the mean flow field. Also, the high-resolution salinity field in the northernmost part of the sections (between ATLAS buoys) displays the western part of the CVFZ. A fresh view is provided by the simultaneous velocity and salinity maps from the equator to the CVFZ region.

The PIRATA ship data described here are invaluable to complete the investigations using the high-resolution timeseries from the ATLAS systems. However, measurements during the fall season are still missing. The western tropical Atlantic still needs more detailed direct velocity observations, mainly in the tropical-subtropical band, a key region to climate research. The observational discussion presented in this note are presently

being subject of high-resolution ocean modeling at CPTEC/INPE, and shall contribute to enlarge the picture inferred from the observational evidence presented here.

References

Arhan, M., H. Mercier, B. Bourlès, and Y. Gouriou (1998), Hydrographic sections across the Atlantic at 7°30N and 4°30S, *Deep-Sea Res. I*, *45*, 829–872.

Arhan, M., A. M. Treguier, B. Bourlés, and S. Michel (2006), Diagnosing the Annual Cycle of the Equatorial Undercurrent in the Atlantic Ocean from a General Circulation Model, *J. Phys. Oceanogr.*, *36*, 1502–1522.

Austin, T. S. (1963), Equalant, *Am. Inst. Biol. Sci. Bull.*, *13*(5), 46–48.

Bourlès, B., Y. Gouriou, and R. Chuchla (1999a), On the circulation in the upper layer of the western equatorial Atlantic, *J. Geohys. Res., C*, *104*(C9), 21,151–21,170.

Bourlès, B., R. L. Molinari, E. Johns, W. D. Wilson, and K. D. Leaman (1999b), Upper layer currents in the western tropical North Atlantic (1989-1991), *J. Phys. Oceanogr.*, *104*(C1), 1361–1375.

Bourlès, B., M. D'Orgeville, G. Eldin, Y. Gouriou, R. Chucla, Y. DuPenhoat, and S. Arnault (2002), On the evolution of the thermocline and subthermocline eastward currents in the Equatorial Atlantic, *Geophys. Res. Lett.*, *29*(16), 1785, doi: 10.1029/2002GL015098.

Brown, W. S., W. E. Johns, K. D. Leaman, J. P. McCreary, R. L. Molinari, P. L. Richardson, and C. Rooth (1992), A Western Tropical Atlantic Experiment (WESTRAX), *Oceanography*, *5*(1), 73–77.

Cochrane, J. D. (1963), Equatorial Undercurrent and related currents off Brazil in March and April 1963, *Science*, pp. 669–671.

Firing, E., J. Ranada, and P. Caldwell (1995), *Processing ADCP Data with the CODAS Software System Version 3.1.*, Joint Institute for Marine and Atmospheric Research/NODC, University of Hawaii, USA.

Garzoli, S. L. (1992), The Atlantic North Equatorial Countercurrent: Models and Observations, *J. Geophys. Res.*, *97*(C11), 17,931–17,946.

Goes, M., R. Molinari, I. C. A. Silveira, and I. Wainer (2005), Retroflections of the North Brazil Current during February 2002, *Deep-Sea Res. I*, *52*, 647–667, doi:10.10.16/j.dsr.2004.10.010.

Inui, T., A. Lazar, P. Malanotte-Rizzoli, and A. Busalacchi (2002), Wind stress effects on subsurface pathways from the subtropical to tropical Atlantic, *J. Phys. Oceanogr.*, *32*, 2257–2276.

Jochum, M., and P. Malanotte-Rizzoli (2003), On the generation of North Brazil Current rings., *J. Mar. Res.*, *61*(2), 147–162.

Jochum, M., and P. Malanotte-Rizzoli (2004), A new theory for the generation of equatorial subsurface countercurrents., *J. Phys. Oceanogr.*, *34*, 755–771.

Katz, E. J. (1987), Seasonal response of the sea surface to the wind in the equatorial Atlantic, *J. Geophys. Res.*, *92*, 1885–1893.

Katz, E. J., and S. Garzoli (1984), Thermocline displacement across the Atlantic North Equatorial Countercurrent during 1983, *Geophys. Res. Lett.*, *11*(8), 737–740.

Klein, B., and G. Siedler (1995), Isopycnal and Diapycnal Mixing at the Cape Verde Frontal Zone, *J. Phys. Oceanogr.*, *25*, 1771–1787.

Lazar, A., T. Inui, P. Malanotte-Rizzoli, A. Busalacchi, L. Wang, and R. Murtugudde (2002), Seasonality of the ventilation of the tropical Atlantic thermocline in an ocean general circulation model, *J. Geophys. Res.*, *107*(C8), 3104-3121.

Lee, S.-K., and G. T. Csanady (1999), Warm water formation and escape in the upper tropical Atlantic Ocean: A literature review, *J. Geophys. Res.*, *104*(C12), 29,561–29,571.

Lozier, M. S., W. B. Owens, and R. G. Curry (1995), The climatology of the North Atlantic, *Prog. Oceanog.*, *36*, 1–44.

Luedemann, E. F. (1967), Preliminary results of drift-bottle releases and recoveries in the western tropical Atlantic, *Bolm. Inst. Oceanogr.*, *16*, 13–22.

Malanotte-Rizzoli, P., K. Hedstrom, H. Arango, and D. Haidvogel (2000), Water mass pathways between the subtropical and tropical ocean in a climatological simulation of the North Atlantic ocean circulation, *Dyn. Atmos. Oceans.*, *32*, 331–371.

Mayer, D. A., and R. H. Weisberg (1993), A Description of COADS Surface Meteorological Fields and the Implied Sverdrup Transports for the Atlantic Ocean from 30S to 60N., *J. Phys. Oceanogr.*, *23*, 2201–2221.

McCreary, J. P., P. Lu, and Z. Yu (2002), Dynamics of the Pacific subsurface countercurrents, *J. Phys. Oceanogr.*, *32*, 2379–2404.

Metacalf, W. G. (1968), Shallow currents along the northeastern coast of South America, *J. Mar. Res.*, *26*, 232–243.

Metacalf, W. G., and M. C. Staculp (1967), Origen of the Atlantic Equatorial Undercurrent, *J. Geophys. Res.*, *22*, 4959–4975.

Molinari, R. L., B. Voituriez, and P. Duncan (1981), Observations in the subthermocline undercurrent of the equatorial South Atlantic Ocean: 1978-1980, *Oceanol. Acta*, *4*, 451–456.

Onken, R., and B. Klein (1991), A Model of Baroclinic Instability and Waves between Ventilated Gyre and the Shadow Zone of the North Atlantic Ocean, *J. Phys. Oceanogr.*, *21*, 53–67.

Perez-Rodriguez, P., J. L. Pelegri, and A. Marrero-Diaz (2001), Dynamical characteristics of the Cape Verde frontal zone, *Sci. Mar.*, *65*(1), 241–250.

Schott, F. A., P. Brandt, M. Hamann, J. Fischer, and L. Stramma (1995), On the boundary flow off Brazil at 5-10°S and its connection to the interior tropical Atlantic, *J. Geophys. Res.*, *100*(C12), 24,745–24,760.

Schott, F. A., J. Fischer, and L. Stramma (1998), Transports and Pathways of the Upper-Layer Circulation in the Western Tropical Atlantic, *J. Phys. Oceanogr.*, *28*, 1904–1928.

Servain, J. M., A. J. Busalacchi, M. J. McPhaden, A. D. Moura, G. Reverdin, M. Vianna, and S. Zebiak (1998), A Pilot Research Moored Array in the Tropical Atlantic, *Bull. Am. Meteor. Soc.*, *79*, 2019–2031.

Spall, M. A. (1992), Rossby Wave Radiation in the Cape Verde Frontal Zone, *J. Phys. Oceanogr.*, *22*, 796–807.

Stramma, L., and F. Schott (1999), The mean flow field of the tropical Atlantic Ocean, *Deep Sea Research II*, *46*, 279–303.

Stramma, L., S. Juttl, and J. Schafstall (2005a), Water masses and currents in the upper tropical northeast Atlantic off northwest Africa, *J. Geophys. Res.*, *110*(C12006), doi: 10.1029/2005JC002939.

562 Stramma, L., M. Rhein, P. Brandt, M. Dengler, C. Boning, and M. Walter (2005b), Upper
563 ocean circulation in the western tropical Atlantic in boreal fall 2000, *Deep Sea Research*
564 *I*, *52*, 221–240, doi:10.1016/j.dsr.2004.07.021.
565 Urbano, D. F., M. Jochum, and I. C. A. Silveira (2006), Redescovering the second core of
566 the Atlantic NECC, *Ocean Model.*, *12*, 1–15, doi:10.1016/j.ocemod.2005.04.003.
567 Vangriesheim, A., C. Bournot-Marec, and A.-C. Fontan (2003), Flow variability near the
568 Cape Verde frontal zone (subtropical Atlantic Ocean), *Oceanologica Acta*, *26*, 149–159.
569 Wilson, W. D., E. Johns, and R. L. Molinari (1994), Upper layer circulation in the western
570 tropical North Atlantic Ocean during August 1989, *J. Geophys. Res.*, *99*(C11), 22,513–
571 22,523.
572 Zang, D., M. J. McPhaden, and W. E. Johns (2003), Observational Evidence for Flow
573 between the Subtropical and Tropical Atlantic: The Atlantic Subtropical Cells, *J. Phys.*
574 *Oceanogr.*, *33*, 1783–1797.

Table 1. Summary of Brazilian PIRATA cruises, dates and ADCP/CTD data types.

Cruise	Alias	Boreal Season	Section	Data type
PIRATA BR I [a]	JAN1998	winter	15N-4N , 38°W	CTD
PIRATA BR II	FEB1999	winter	15°N-3°S , 38°W	Transect/CTD
PIRATA BR III	MAR2000	winter	15°N-2°S , 38°W	Transect/CTD
PIRATA BR IV	APR2001	spring	15°N-3°S , 38°W	VM-DAS/CTD
PIRATA BR V	APR2002	spring	15°N-3°S , 38°W	VM-DAS/CTD
PIRATA BR VI	JUL2003	summer	15°N-3°S , 38°W	VM-DAS/$CTDO_2$
PIRATA BR VII	JUL2004	summer	15°N,38°W- 3°S,35°W	VM-DAS/$CTDO_2$ [b]
PIRATA BR VIII	JUL2005	summer	15°N-2°S , 38°W	VM-DAS/$CTDO_2$ [b]

[a] Will not be used here.

[b] $CTDO_2$ at ATLAS sites only.

Table 2. Current transports in Sverdrups (Sv) at 38°W for each PIRATA cruise.

Cruises	EUC	sNECC	nNECC	NECC	nSEC	NEUC
Limits of	2S-3N	3-8N	8-14N	3-14N	0-8N	3-7N
integration	24-250m	24-120m	24-250m	24-120m	24-120m	≈70-250m
FEB1999	23.5*	7.6	4.6	10.5	-1.1	8.9
MAR2000	29.0*	5.3	3.6	7.4	-2.4	5.6
APR2001	31.8	1.0	–	1.0	-7.5	0.7*
APR2002	10.7*	3.4	2.1	4.0	-14.3	1.0
JUL2003	14.3	13.1	4.6	17.9	-17.3	3.4
JUL2004	17.9	4.4	7.4	9.8	-13.8	3.6
JUL2005	21.2	11.4	2.8	12.9	-4.8	5.4*

* Incomplete sampling of the current domain leading to underestimated values.

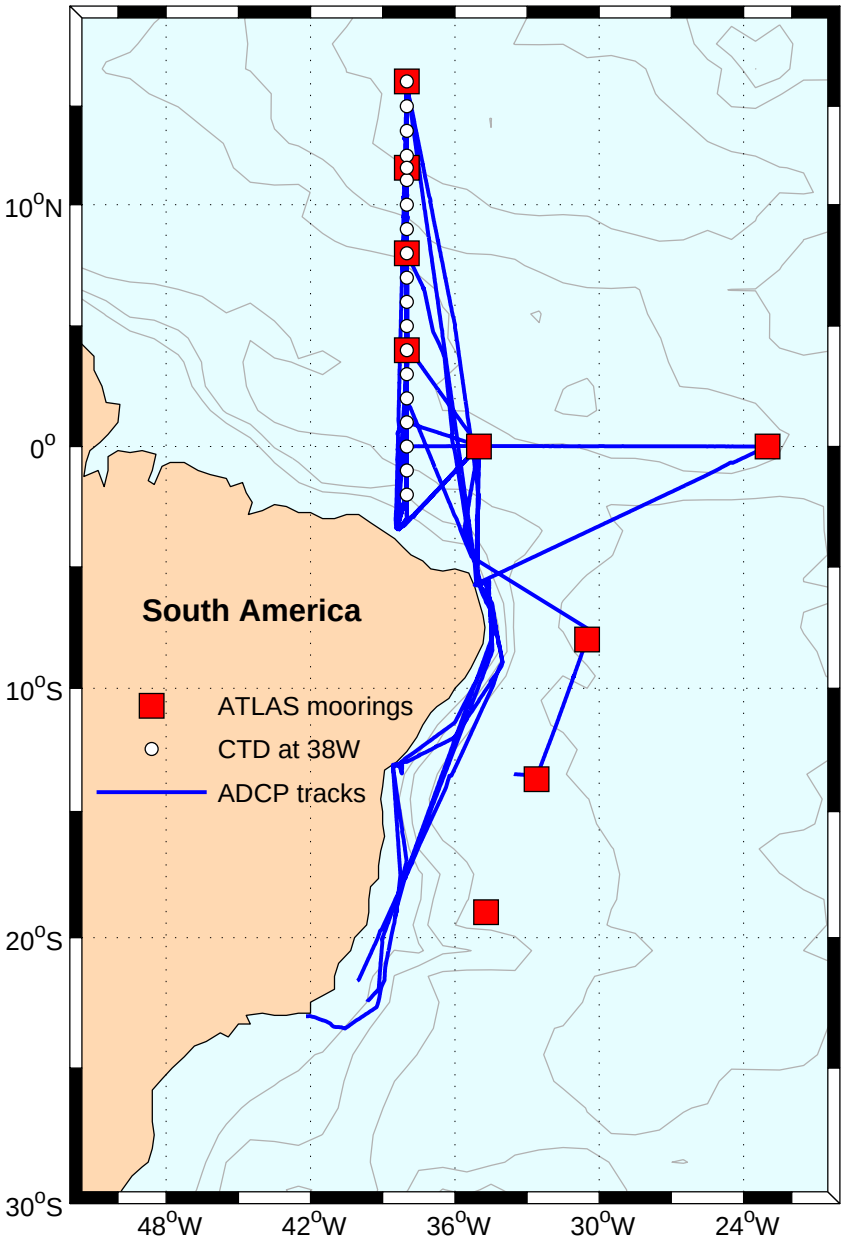

Figure 1. Western PIRATA array. ATLAS moorings (squares), CTD stations along 38°W (circles) and VM-ADCP Brazilian tracks (lines). The gray contours show the bathymetry.

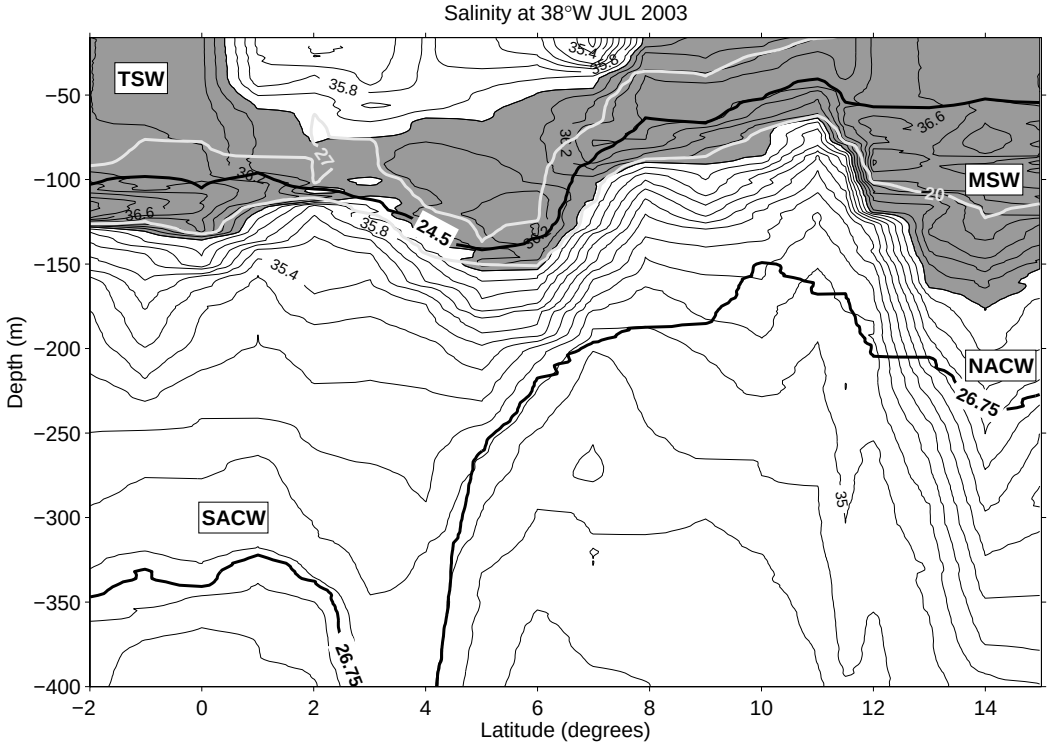

Figure 2. The water masses along 38°W for July 2003: Tropical Surface Water (TSW); South Atlantic Central Water (SACW); Salinity Maximum Water (SMW); and North Atlantic Central Water (NACW). Contours are salinity with gray shade for values over 36 psu. Density surfaces of 24.5 and 26.75 Kg m^{-3} (thick black lines) and temperature surfaces of 20°C, 25°C, and 27°C were superimposed (gray lines).

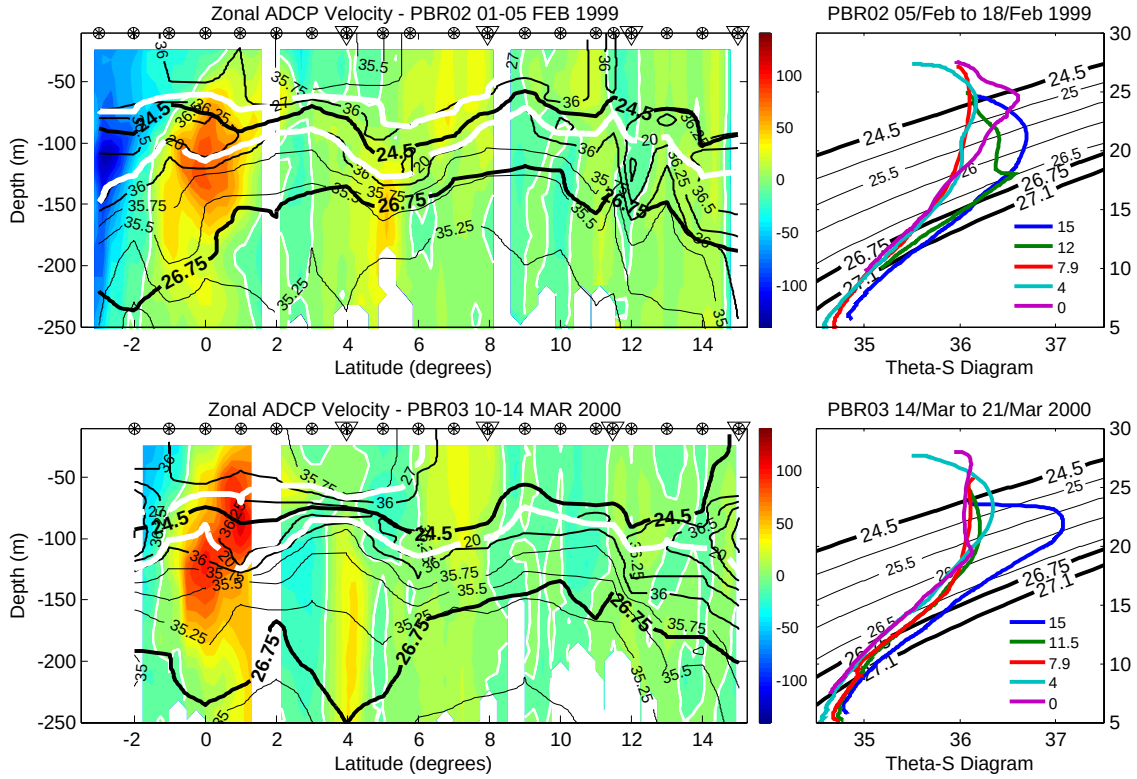

Figure 3. Vertical maps along 38°W (right) and correspondent Theta-S diagrams (left) for winter cruises. Shaded colors show the ADCP zonal velocity component in cm s^{-1}. Positive (eastward) velocity in red and negative (westward) velocity in blue, with zero velocity in thin white lines. Overlaid are salinity (black thin lines) with contour interval of 0.25, temperatures of 20°C and 27°C (white thick lines), and densities of 24.5 and 26.75 Kg m^{-3} (black thick lines). On the top, circles are the CTD stations and triangles are ATLAS moorings. The Theta-S legend displays the latitudes in degrees.

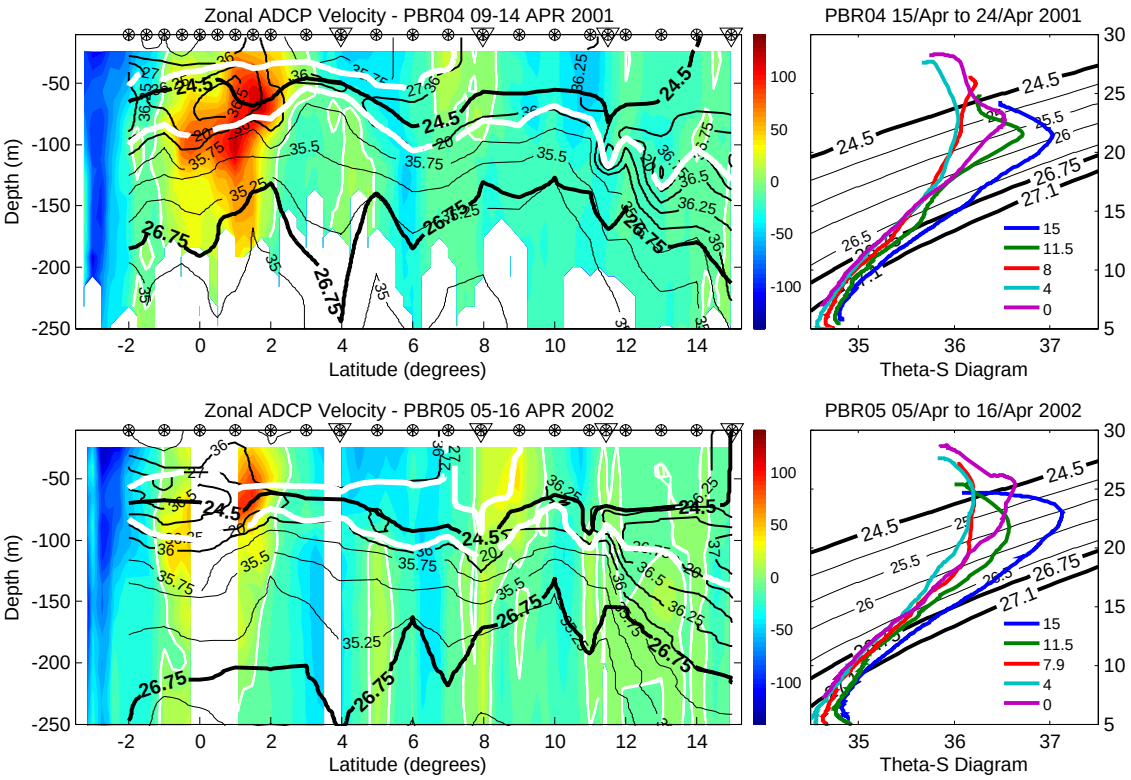

Figure 4. Same of Figure 3 but for spring.

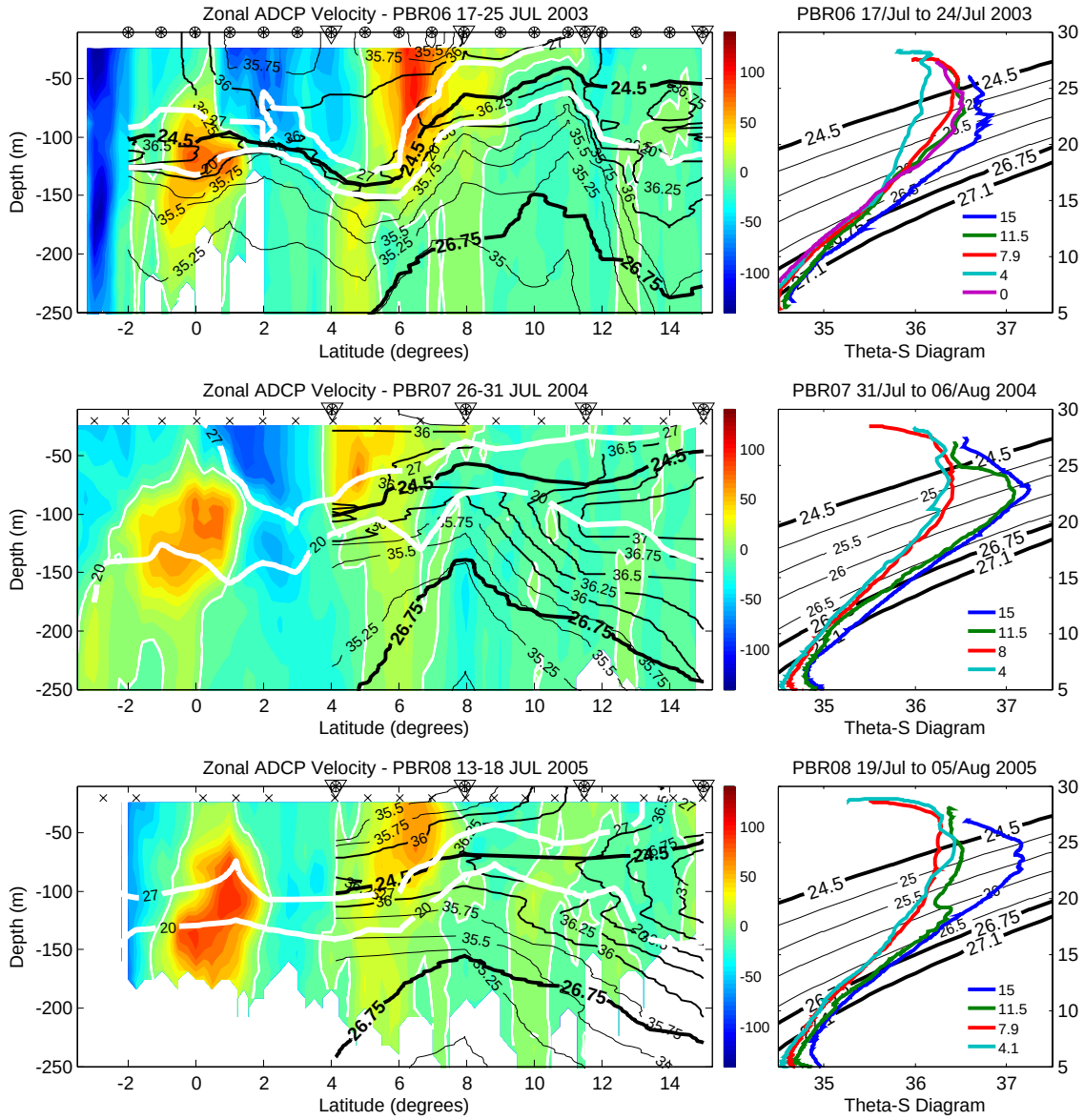

Figure 5. Same of Figure 3 but for summer.

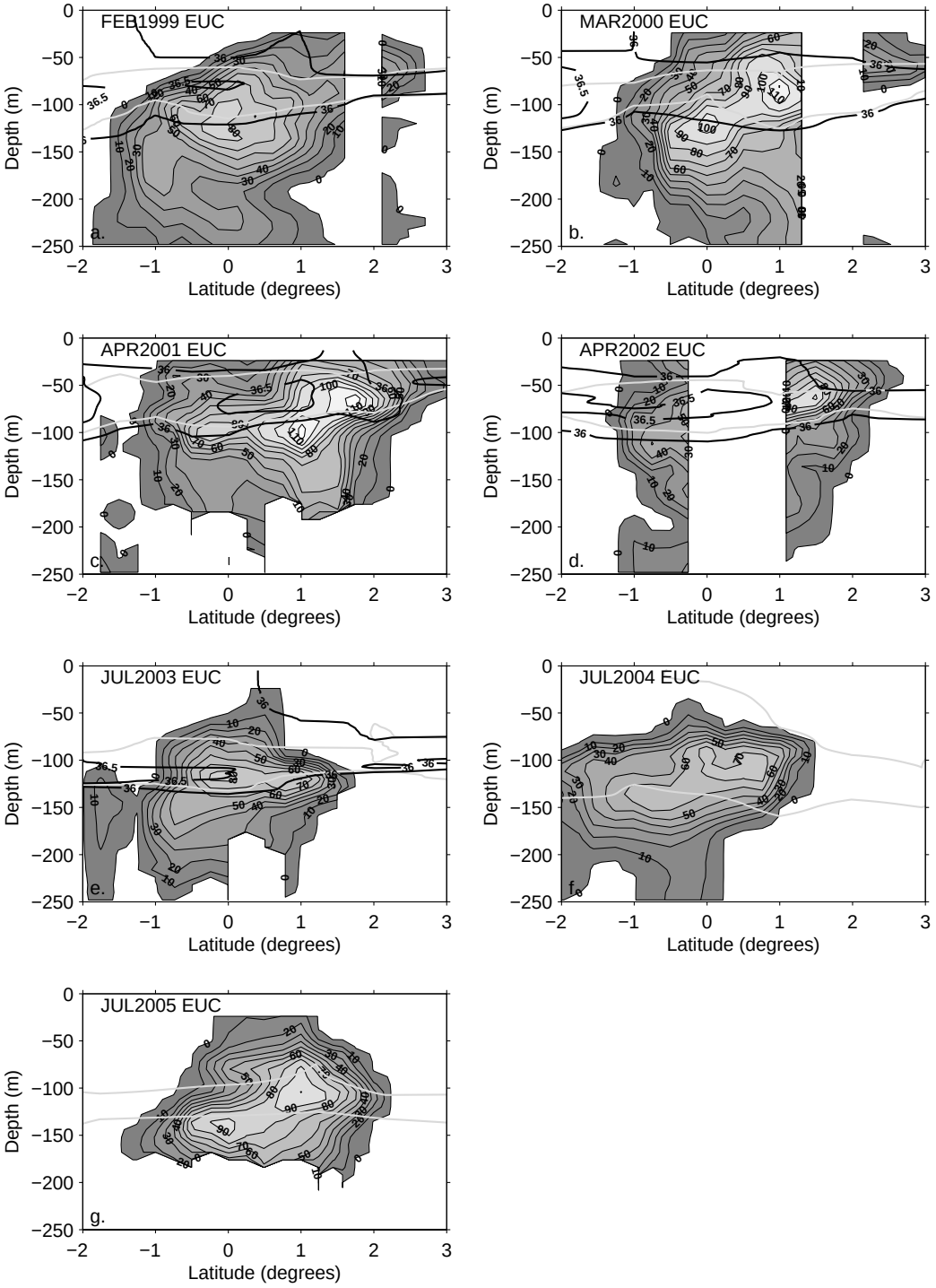

Figure 6. Positive velocity section in the EUC limits. Overlaid is the salinity contours of 36 and 36.5, and temperature contours of 27°C (shallower) and 20°C.

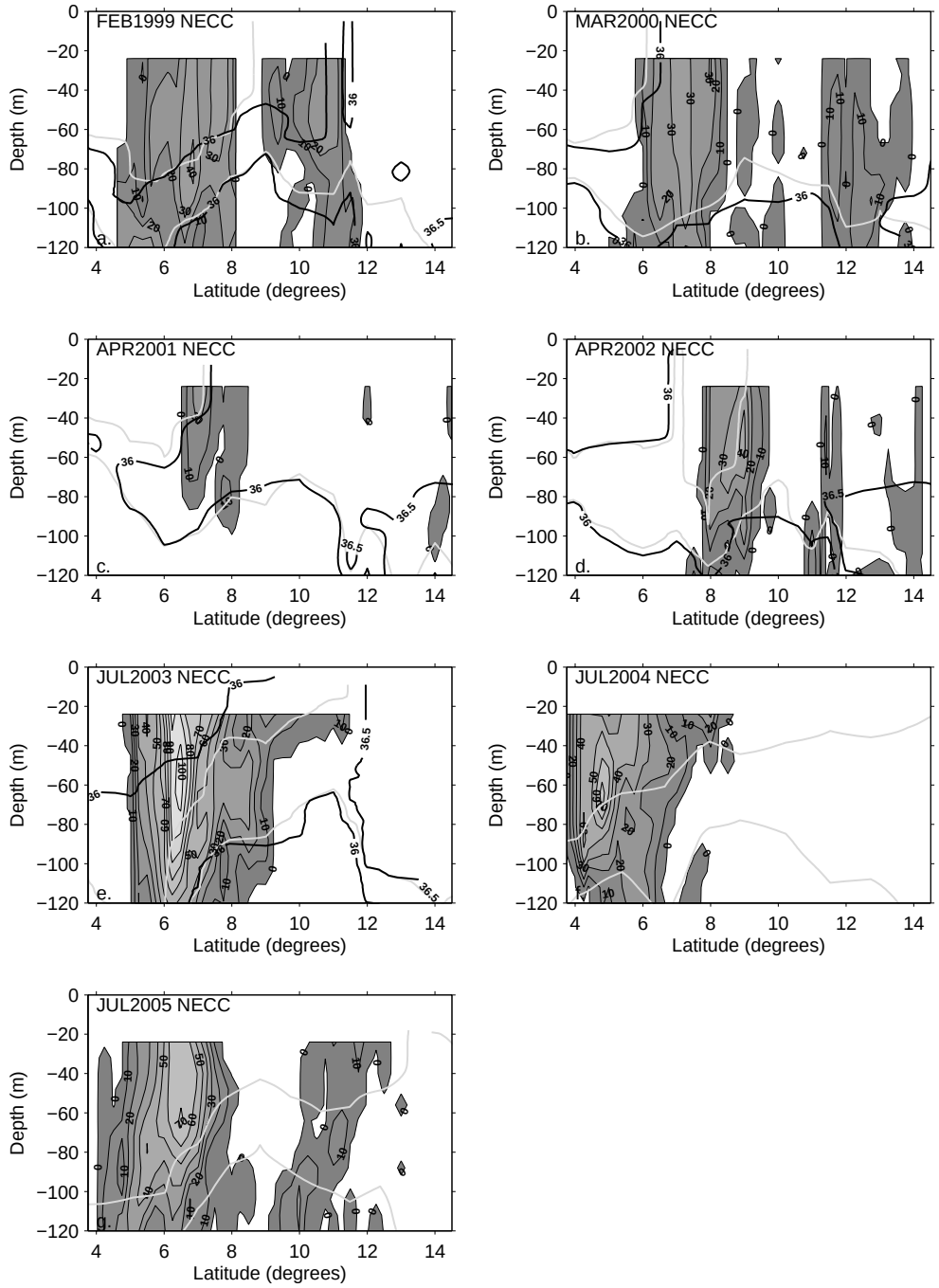

Figure 7. Positive velocity section in the NECC limits. Overlaid is the salinity contours of 36 and 36.5 (thick black contours), and temperature contours of 27°C (shallower) and 20°C (light gray contours). In f and g, there is no high-resolution salinity available, while temperature are from XBT.

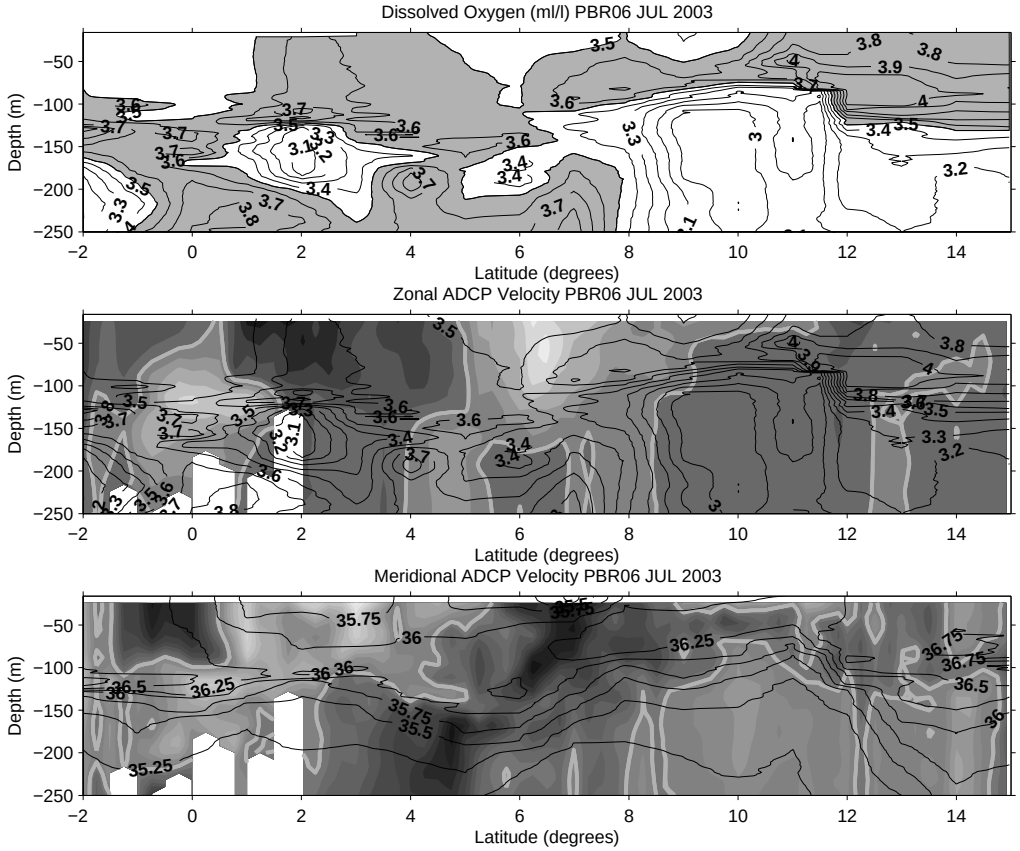

Figure 8. Vertical distribution of dissolved oxygen, salinity and velocity along 38°W for July 2003. (a) Contours of dissolved oxygen; values above 3.5 ml l^{-1} were shaded in gray. (b) dissolved oxygen superimposed on the zonal velocity. Dark (light) shades are westward (eastward) flow. (c) salinity superimposed on the meridional velocity. Dark (light) shades are southward (northward) flow; thick gray line is zero.